CARBON DIOXIDE FLUX AND CARBON AND HELIUM ISOTOPIC COMPOSITION OF SOIL GASES ACROSS THE FORGE SITE AND OPAL MOUND FAULT, UTAH

by Kristen Rahilly[1], Stuart Simmons[2,3], and Tobias P. Fischer[1]

[1] Department of Earth and Planetary Sciences, University of New Mexico, Albuquerque, New Mexico
[2] Energy & Geoscience Institute, University of Utah, Salt Lake City, Utah
[3] Department of Chemical Engineering, University of Utah, Salt Lake City, Utah

Link to supplemental data download: https://ugspub.nr.utah.gov/publications/misc_pubs/mp-169/mp-169-i.zip
Appendix

Miscellaneous Publication 169-I
Utah Geological Survey
a division of
UTAH DEPARTMENT OF NATURAL RESOURCES

This paper is part of *Geothermal Characteristics of the Roosevelt Hot Springs System and Adjacent FORGE EGS Site, Milford, Utah*. https://doi.org/10.34191/MP-169

Bibliographic citation:

Rahilly, K., Simmons, S., and Fischer, T.P., 2019, Carbon dioxide flux and carbon and helium isotopic composition of soil gases across the FORGE site and Opal Mound fault, Utah, *in* Allis, R., and Moore, J.N., editors, Geothermal characteristics of the Roosevelt Hot Springs system and adjacent FORGE EGS site, Milford, Utah: Utah Geological Survey Miscellaneous Publication 169-I, 16 p., 1 appendix, https://doi.org/10.34191/MP-169-I.

CARBON DIOXIDE FLUX AND CARBON AND HELIUM ISOTOPIC COMPOSITION OF SOIL GASES ACROSS THE FORGE SITE AND OPAL MOUND FAULT, UTAH

by Kristen Rahilly, Stuart Simmons, and Tobias P. Fischer

ABSTRACT

Surface measurements of soil carbon dioxide flux and isotopic composition across the Utah FORGE site and Roosevelt Hot Springs are used to assess the potential of hydrothermal activity west of the N-S trending Opal Mound fault. Carbon dioxide flux surveys were made in June 2017 and January 2018 using a PP Systems EGM 5 portable carbon dioxide analyzer. A total of 317 flux measurements were made across the FORGE site with 0.16 km spacing between points oriented along east-west and north-south grid lines. Additionally, 626 total flux measurements were made in east-west transects across the Opal Mound fault and across the Mineral Mountains West fault scarps approximately 2 km SW of the Opal Mound fault.

Individual flux points are categorized as either background vegetation or elevated values using the statistical Sinclair method. Interpolation of flux for both the FORGE site and across faulted areas outside the FORGE site is performed using Empirical Bayesian Kriging in the Geostatistical Analyst toolbox of ArcGIS. Variance above statistical background is then calculated to reveal regions with elevated carbon dioxide flux. The extrapolated soil flux map shows the FORGE site does not contain carbon dioxide flux values above regional vegetation background values, within analytical error. Regions of flux values elevated above statistical background occur near and to the east of the Opal Mound fault.

Soil carbon dioxide gas samples were collected in 1 liter Tedlar bags for measurement of $\delta^{13}C$ isotopic composition using a Thermo Fisher Delta Ray Isotope Ratio Infrared Spectrometer (IRIS) instrument. Samples of soil carbon dioxide were collected from both high and low flux points within the FORGE site as well as from vegetation points outside the FORGE site and across the Opal Mound fault. The isotopic composition of points taken on the FORGE site cluster with samples taken from vegetation points outside the FORGE site. Several soil carbon dioxide gas samples collected east of the Opal Mound fault may contain evidence of a magmatic source.

Finally, diffusion samplers were deployed in piezometers to characterize the helium isotope compositions of soil gases. Over the FORGE site, air corrected R/Ra values range between 0.1 and 1.0 whereas over Roosevelt Hot Springs, east of the Opal Mound fault, R/Ra values are up to 2.2. These He isotopic measurements along with flux measurements provide unambiguous geochemical evidence that the FORGE site is isolated from convective hydrothermal fluid flow and magmatic influences associated with the Roosevelt Hot Springs system.

INTRODUCTION

The Utah Frontier Observatory for Research in Geothermal Energy (FORGE) Enhanced Geothermal System (EGS) site is located in southwestern Utah (Figure 1) approximately 16 km northeast of Milford, Utah (e.g., Allis et al., 2016; Simmons et al., 2018). The site is west of the Mineral Mountains in the southeast part of the Basin and Range province, west of the transition zone into the Colorado Plateau province. The FORGE site is underlain by Quaternary through Tertiary-age basin fill overlying basement rock that includes Miocene granitoids and Precambrian gneiss. Beneath the FORGE site, depth to basement varies from 300 m to 1 km along a gentle west-dipping basement-basin fill contact (Hardwick et al., 2019; Miller et al., 2019; Jones et al., 2019).

Approximately 2 km east of the FORGE site lies the north-trending Opal Mound fault, a high-angle normal fault that was last seismically active during the late Pleistocene (Nielson et al., 1986; Knudsen et al., 2019). The Opal Mound fault has been the site of episodic discharge of deep thermal water. Discharge of thermal water has produced the silica sinter mound at the southern end of the Opal Mound fault as well as a series of sinter-cemented fan deposits along the trace of the fault (Moore and Nielson, 1994; Lynne et al., 2005). The Opal Mound fault forms the western boundary of the Roosevelt Hot Springs hydrothermal system (Nielson et al., 1986; Allis and Larsen, 2012; Allis et al., 2016; Simmons et al., 2018). Roosevelt Hot Springs is located within the Sevier thermal anomaly, a region of high heat flow that includes many of the geothermal systems within southwestern Utah (Blackett, 2007; Simmons et al., 2015). Roosevelt Hot Springs system reservoir fluids

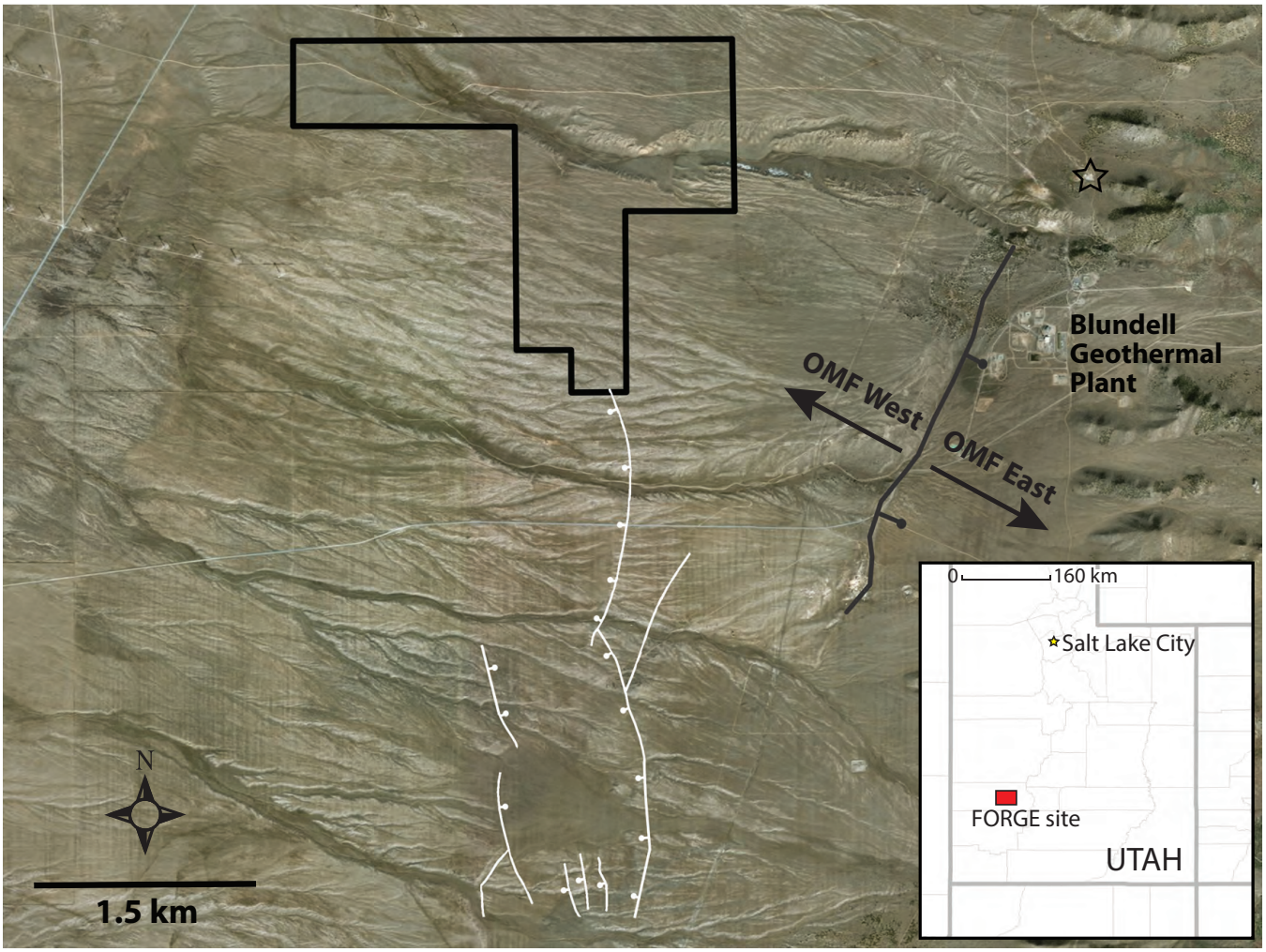

Figure 1. *Location of FORGE site (black polygon), Opal Mound fault (dark gray line), Mineral Mountains West fault scarps (white lines), and Roosevelt Hot Springs (black star). Opal Mound fault (OMF) West and East sampling areas indicated by black arrows. Location of FORGE site (inset map).*

have a maximum temperature of 260°C and are used to generate power at the Blundell power plant (33 MWe), which has operated continuously since 1984 (e.g., Faulder, 1991; Allis and Larsen, 2012). Fumarole gases from Roosevelt Hot Springs have high $^{3}He/^{4}He$ ratios with an air corrected value of R/Ra = 2.25, indicating a component of mantle helium (Kennedy and van Soest, 2007).

To better constrain deep-seated gas near the FORGE site, a soil gas carbon dioxide (CO_2) flux survey with accompanying soil gas $\delta^{13}C$ isotopic compositional analysis was performed in June 2017 and January 2018. In addition, a helium isotope soil gas survey was performed in November 2017, using diffusion samplers that are commonly used for sampling dissolved noble gases in the phreatic zone (e.g., Sanford et al., 1996; Gardner and Solomon, 2009; Dame et al., 2015). The goal was to constrain helium signatures, representing a range of values (i.e., radiogenic crustal R/Ra ~0.1, air R/Ra = 1, Roosevelt Hot Springs R/Ra ~2), in the shallow part of the vadose zone (e.g., Wannamaker et al., 2017).

SOIL CO_2 FLUX MEASUREMENTS

High rates of soil CO_2 flux have been consistently measured across a variety of active and quiescent volcanic areas as well as in geothermal reservoirs (Chiodini et al., 1998; Lewicki and Oldenburg, 2005). CO_2 is the most abundant non-condensable gas emitted by most geothermal systems and, due to its moderate solubility in water, is an ideal indicator of hydrothermal and magmatic activity at depth. In geothermal and volcanic regions, surficial measurements of CO_2 flux above background levels indicate sufficiently permeable pathways to allow transport of deeply-sourced CO_2 (Lewicki and Oldenburg, 2005). These

pathways could include interconnected pore spaces or faults/fractures of various geometries and dimensions (Lewicki and Oldenburg, 2005; Peiffer et al., 2014; Lee et al., 2016). The CO_2 flux measured at the surface may be contributed by multiple sources and analyses should distinguish between background (biogenically or atmospherically-sourced CO_2) and magmatic/deeply-sourced CO_2 (Chiodini et al., 1998; Lewicki and Oldenburg, 2005). By combining flux measurements with $\delta^{13}C$ analyses, the sources for soil CO_2 can be identified (Chiodini et al., 2008; Parks et al., 2013; Lee et al., 2016). In geothermal or volcanic areas, CO_2 samples reaching the surface will be either purely magmatic, purely biogenic, or mixtures between the two based on isotopic composition and flux. For a prospective EGS reservoir with sealed, low-permeability basement rock, we expect surficial CO_2 to be within background values (Peiffer et al., 2014).

METHODS

We used a PP Systems Environmental Gas Monitor (EGM) 5 with soil respiration (accumulation) chamber to measure soil CO_2 flux with a 317-point gridded survey across the FORGE site and at an additional 626 points in transects across the Opal Mound fault and south of the FORGE site in June 2017 and January 2018 (Figure 2). Individual point measurements have a consistent spacing of 0.16 km in the FORGE site. Points outside of the FORGE site were acquired using an adaptive sampling technique as described by Werner and Brantley (2003). An adaptive sampling technique uses an initial coarser gridded survey but allows for smaller spacing between points if an anomalously high flux is measured (Werner and Brantley, 2003).

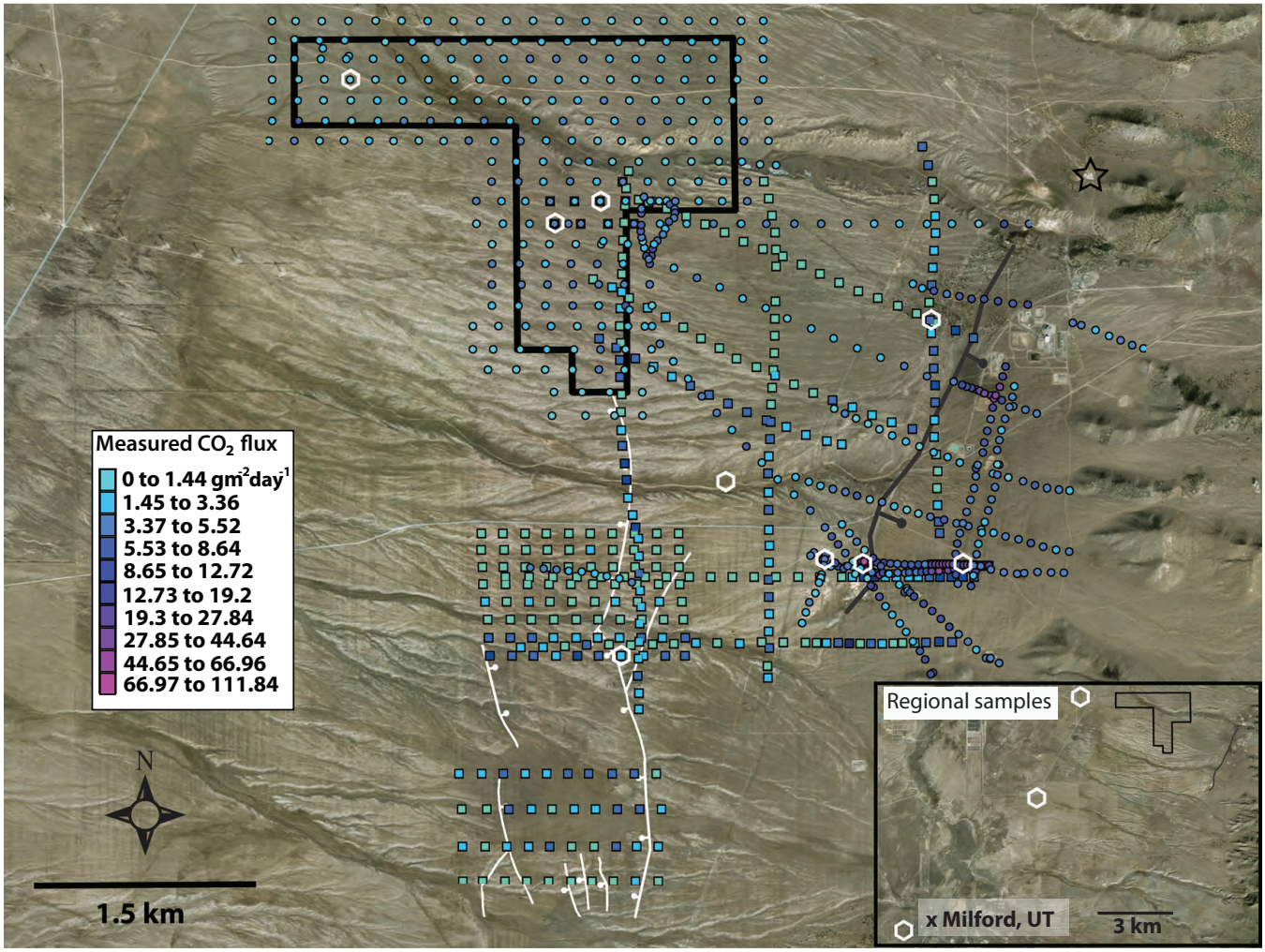

Figure 2. *Actual CO_2 flux measurements from June (circles) and January (squares) across the FORGE site (black polygon), Opal Mound fault (dark gray line), and Mineral Mountains West fault scarps (white lines). White hexagons are the locations of gas samples collected for $\delta^{13}C$ isotope composition analysis. The locations of regional gas samples are shown in inset. Roosevelt Hot Springs is the black star.*

To measure soil gas CO_2 flux, the EGM 5 with soil respiration chamber is placed securely on a soil surface, creating a seal (Figure 3A). Soil gas is then drawn up into the chamber from the soil surface using a rotary air sampling pump. The gas is passed through an infrared analyzer which measures the concentration of CO_2 and then pumped back into the chamber to create a closed system. The rate of change in CO_2 concentration over the entire 124 second measurement period is then determined using a linear fit calculation to obtain the CO_2 flux from that location (PP Systems, 2016). Once the measurement has been made, the flux value is recorded in g $CO_2/m^2/hr$.

For $\delta^{13}C$ isotope composition analyses, gas samples were collected from points with both high and low soil CO_2 flux (Figure 2). Soil gas samples were collected by connecting a 1 liter Tedlar® bag to the gas outlet of the EGM 5 analyzer (Figure 3B). In the FORGE site, soil gas samples were collected from both low flux and high flux points to evaluate whether higher flux rates are related to more deeply sourced CO_2.

Soil gas samples were also collected on both sides of the Opal Mound fault. Regional vegetation samples were also collected 1 to 15 km outside the FORGE site or Opal Mound fault areas (Figure 2 inset). Finally, three atmospheric gas samples were collected to determine the value of ambient air that may mix with our soil samples at the soil-air interface.

Tedlar bag gas samples were measured for $\delta^{13}C$ isotope composition of CO_2 the same day they were collected using a Thermo Fisher Delta Ray Isotope Ratio Infrared Spectrometer (IRIS) located at the field base station. The Delta Ray IRIS measures the infrared spectra of carbon isotopes to determine concentration and isotope composition (Rizzo et al., 2014; Fischer and Lopez, 2016). Samples of CO_2 can be measured from air-like concentrations up to pure CO_2. Gas samples above 3500 ppm CO_2 require dilution using the Thermo Fisher Xpand dilution box with incremented dilution capillaries.

CO_2 flux measured in June and January may be alternatively affected by weather and/or frozen ground and must be normalized to produce consistent data (Lewicki et al., 2003; Lewicki et al., 2005). For this reason, we plot variance above biogenic background flux rather than absolute flux. To do this, we have to calculate the background biogenic flux for both the June and January sets of measurements using the statistical population distribution method for geochemical data described by Sinclair (1974). This method calculates a maximum flux threshold for background CO_2 related to the processes associated with biogenically-sourced CO_2 (Chiodini et al., 1998). Any value above this maximum background is classified as anomalous and thus related to geothermal processes (Lewicki and Oldenburg, 2005).

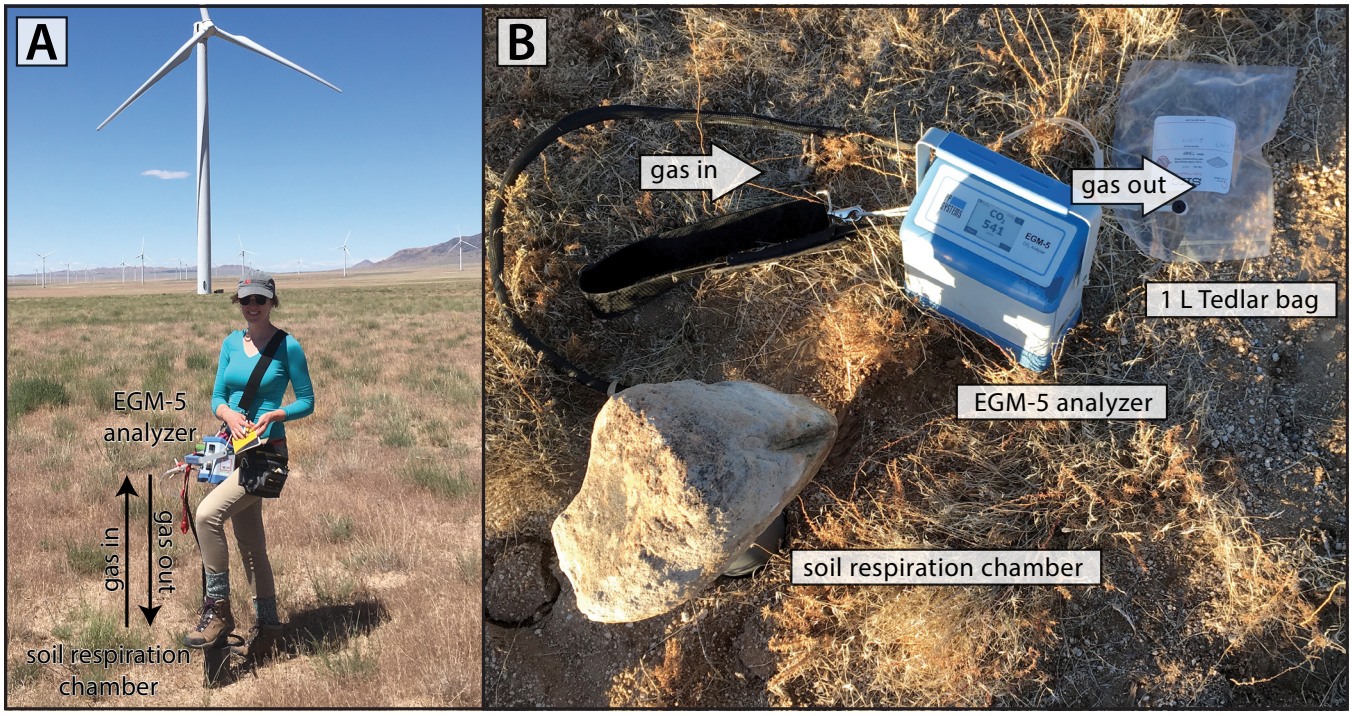

Figure 3. (A) *Field deployment of EGM 5 instrument with soil respiration chamber.* ***(B)*** *EGM 5 with Tedlar bag connected to gas out port for collection of soil gas samples.*

To normalize the flux measurements to variance above biogenic background using the Sinclair method, the cumulative probability distribution of both the June (Figure 4A) and January (Figure 4B) datasets was plotted separately against flux per day on a logarithmic plot. Based on the chosen inflection point along the distribution curve, the January dataset (Figure 4B) is composed of two populations: 1) 95% of the data are in a background (biogenic) flux population and 2) the remaining 5% are in an elevated (geothermal) flux population.

These values were chosen based on the inflection point at the cumulative probability of 5% and a check of the data was completed by adding flux measurements at defined probability intervals by using the following equation: (0.05*elevated) + (0.95*background) = mixture value (yellow triangles in Figure 4). If the dataset distribution has been correctly estimated, the mixture values will lie on the true data curve (gray points in Figure 4B). For the January dataset, the mixture values fit the true data and suggest that our proportions are correct (Figure 4B). The maximum threshold for biogenic CO_2 flux for the January dataset is 5.48 $gm^{-2}day^{-1}$ (green horizontal line in Figure 4B).

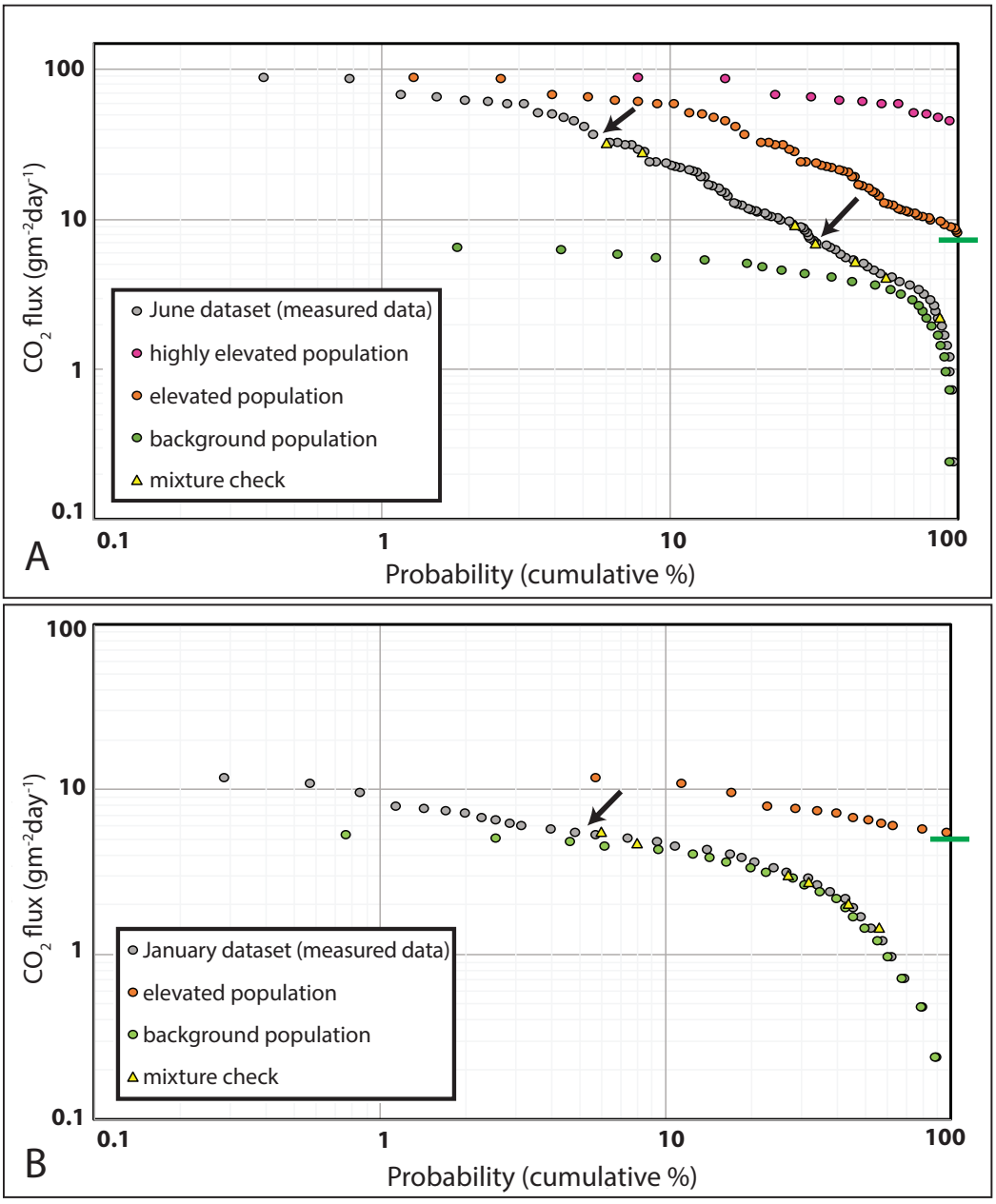

Figure 4. (A) *Population distribution of June 2017 CO_2 flux dataset across the FORGE site and Opal Mound fault.* ***(B)*** *Population distribution of January 2018 CO_2 flux dataset across the FORGE site, Opal Mound fault, and Mineral Mountains West fault scarps. Green horizontal lines indicate threshold between background population and elevated population (8.11 $gm^{-2}day^{-1}$ for June 2017; 5.48 $gm^{-2}day^{-1}$ for January 2018). Black arrows indicate chosen inflection points.*

The June flux dataset is more complicated (Figure 4A). A simple distribution of just two populations does not result in mixture check points that lie on the true data curve (gray points in Figure 4A). Therefore, the June dataset is likely comprised of three populations: 1) 65% is a background (biogenic) flux population, 2) 30% is an elevated flux population, and 3) 5% is a highly elevated flux population. The same mixture check was completed for the June dataset and a maximum background threshold of 8.11 $gm^{-2}day^{-1}$ was estimated (green horizontal line in Figure 4A). Note that the Sinclair Method of determining data distribution can be subjective and dependent on the selection of inflection points (Sinclair, 1974). Therefore, it is important to combine our determination of flux thresholds with isotopic analyses to evaluate the spatial distribution of biogenic soil CO_2 and geothermal (elevated) soil CO_2 (Chiodini et al., 2008).

Individual point soil CO_2 flux measurements were interpolated with the Geostatistical Analyst tool in ArcGIS across the entire measured area using Empirical Bayesian Kriging (EBK). EBK accounts for the spatial variance of measurements and is used here due to our use of both a gridded, evenly spaced survey as well as an adaptive survey (Krivoruchko, 2012). EBK is used to interpolate flux values between point measurements for full spatial coverage of the site. To do this, the June and January flux measurements are normalized by combining both datasets into one CO_2 flux map and reporting the variance from maximum background threshold. For the June flux dataset, the variance is calculated between the measured soil CO_2 flux value and the maximum background threshold of 8.11 $gm^{-2}day^{-1}$. For the January flux dataset, the variance is calculated between measured flux values and the calculated background threshold of 5.48 $gm^{-2}day^{-1}$. The variances from June and January are normalized to consider the 1% error of the EGM 5 instrument (PP Systems, 2016). This means that elevated point flux measurements are above statistical background outside analytical error. The variances between statistical background and the flux for each individual point are then combined to make one June-January dataset that is analyzed with the ArcGIS EBK tool. Due to the log-normal distribution of our flux data, we first performed a log-empirical transformation on the data to achieve a normal data distribution. However, before log-transforming our data we had to linearly shift all our data points by a constant value to account for the abundance of negative variance values. EBK analysis was then performed using 50-point subsets over 200 simulations in the Geostatistical Analyst toolkit. After an interpolated flux map was created, we removed the constant linear shift to get true variance above background values.

The helium isotope soil gas survey was performed in November 2017 using diffusion samplers (Figure 5). These samplers were placed into the bottoms of piezometers (2'–3' long and 1" diameter stainless steel tubes), which were inserted into holes dug with an auger tool and backfilled with compacted soil. The piezometer was sealed with a threaded galvanized steel cap. After 9–10 days, the samplers were retrieved and crimped within 1 minute of being exposed to atmosphere to seal the copper capsule. When retrieved, all the piezometers were dry. Three diffusion samplers were tarnished due to H_2S in areas of thermal ground. We also include one sample of deep thermal water from production well 45-3 in this study, collected in a long copper tube in 2015. All of the samples were analyzed for helium and neon isotopes at the University of Utah Dissolved and Noble Gas Lab on a magnetic sector field mass spectrometer, and the precision for these analyses is 1.5% and 2.0%, respectively.

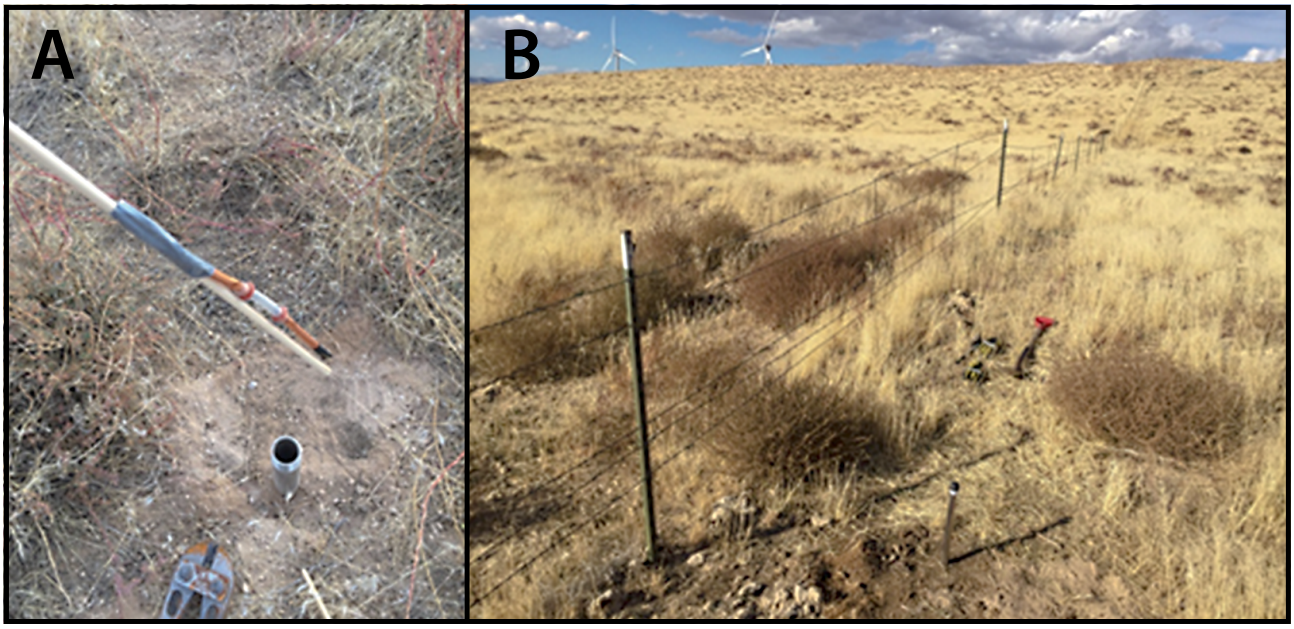

Figure 5. (A) *Copper diffusion sampler taped to the end of a wooden dowel before inserting into stainless steel piezometer tube buried in the ground.* ***(B)*** *Head of capped piezometer tube with copper diffusion sampler inside (not visible).*

Measured $^{3}He/^{4}He$ ratios are normalized using the atmospheric value (Ra = 1.386 x 10^{-6}, Ozima and Podosek, 1983). Using the atmospheric ratio of $^{4}He/^{20}Ne$ (air = 0.318, Ozima and Podosek, 1983), four soil gas samples were corrected for atmospheric contamination with the following expressions:

$$R/Ra\ corrected = (R/Ra-r)/(1-r)$$

$$r = (^{4}He/^{20}Ne)_{air}/(^{4}He/^{20}Ne)_{measured}.$$

As the value of r approaches 1, the corrected values become very sensitive to analytical errors. Hence most of the soil gas samples were not corrected, and they have R/Ra values that are indistinguishable from air.

RESULTS

Soil CO_2 Flux Measurements

Individual soil CO_2 flux measurements made in June 2017 and January 2018 across the FORGE site and Opal Mound fault are shown in Figure 2 (see Appendix[1] for flux point measurements). A summary of dataset statistics is shown in Table 1. For the June dataset, the average and maximum CO_2 flux measured within the FORGE site is less than the average and maximum CO_2 flux measured outside the FORGE site. The maximum CO_2 flux for vegetation east of the Opal Mound fault is nearly 6 times greater than the largest flux measured west of the Opal Mound fault and nearly 14 times larger than the maximum CO_2 flux measured in the FORGE site. The average CO_2 flux for vegetation east of the Opal Mound fault is nearly 3 times larger than the average flux west of the Opal Mound fault and 5 times larger than vegetation measured in the FORGE site. The average CO_2 flux measured across the FORGE site in January is nearly identical to the average measured in June.

Overall, soil CO_2 flux measured in January was less than the CO_2 flux measured in June. This is most likely due to differences in meteorological conditions (Lewicki et al., 2003; Lewicki et al., 2005). During January, low temperatures produced frozen ground conditions (where the ground was observably frosted) during three out of seven field days at the FORGE and Opal Mound fault sites. If pore spaces were filled or partially filled with frozen water, this could decrease soil permeability for the passage of CO_2 to the surface as well as decrease the biogenic production of CO_2 (Elberling, 2003). Additionally, the average daily wind speed for field days in June was 6.6 kilometers per hour versus 4.2 kilometers per hour in January (Western Regional Climate Center, 2018). Lewicki et al. (2003) suggest that small changes in wind speed can result in rapid changes to soil CO_2 flux, possibly due to an increase in advective gas flow.

Compared to other volcanic or geothermal areas, the soil CO_2 flux measured across the FORGE site and Opal Mound fault is lower. Numerous soil CO_2 flux surveys were completed over areas associated with increased desert shrub die-off across the Dixie Valley Geothermal Field in west-central Nevada. These surveys showed a high flux population above 150 $gm^{-2}day^{-1}$ and a maximum flux of 570 $gm^{-2}day^{-1}$. At the Dixie Valley Geothermal Field, a statistical background threshold of 7 $gm^{-2}day^{-1}$ was calculated representing biogenic CO_2 flux across a dry sagebrush landscape similar to the Utah FORGE site (Bergfeld et al., 2001). At the Acoculco caldera hot dry rock geothermal system in Mexico, 95% of the soil CO_2 flux measurements fall within a background population with a mean flux of 18 $gm^{-2}day^{-1}$. The remaining 5% of the flux measurements fall within an elevated range with values up to 39,811 $gm^{-2}day^{-1}$ (Peiffer et al., 2014). The weighted average of these two populations across the entire Acoculco site is then approximately 150 times greater than the average for the FORGE site.

$\delta^{13}C$ Composition of Soil CO_2

Twelve soil CO_2 samples and three air samples were collected across the FORGE site, Opal Mound fault, and regionally in June and January for measurement of $\delta^{13}C$ isotope composition (Figure 2, Table 2). The average $\delta^{13}C$ composition of soil CO_2 within the FORGE site is -12.02‰ for June samples and -12.42‰ for January samples. Only one repeat sample was collected in both June and January for isotopic analysis (samples 3/7). These two samples are within 2% of each other when analytical error is considered. The January sample (sample 7) is heavier than the June sample (sample 3) at -11.876‰ and -12.079‰, respectively. Soil CO_2 collected in vegetation west of the Opal Mound fault has an isotopic composition of -10.41‰ in June and an average isotopic composition of -11.67‰ in January. East of the Opal Mound fault, soil CO_2 samples have an isotopic composition of -10.27‰ in June and -10.00‰ in January. Three regional soil CO_2 samples were collected from points located approximately 1 to 15 km outside of the FORGE site and Opal Mound fault area and have an average isotopic composition of -12.95‰ (Figure 2 inset).

Table 1. *Summary of CO_2 flux dataset statistics from June 2017 and January 2018 inside the FORGE site and across the Opal Mound fault (OMF) compared to other study areas.*

Site	Number of measurements	Maximum CO2 flux ($gm^{-2}day^{-1}$)	Average CO2 flux ($gm^{-2}day^{-1}$)	Background flux ($gm^{-2}day^{-1}$)	Reference
FORGE site 2017	288	8.16	2.02		This study
OMF west vegetation 2017	81	19.2	3.74		This study
OMF east vegetation 2017	226	111.84	10.88		This study
FORGE + OMF total 2017	595			≤ 8.11	This study
FORGE site 2018	29	5.04	2.03		This study
OMF west vegetation 2018	268	10.8	1.98		This study
OMF east vegetation 2018	51	12.24	3.92		This study
FORGE + OMF total 2018	348			≤ 5.48	This study
Dixie Valley Geothermal Field	558	570	32.5	≤ 7.00	Bergfeld et al. (2001)
Acoculco caldera HDR	200	39,811	294.25	mean for background population = 18	Peiffer et al. (2014)

Table 2. *Summary of isotopic and concentration measurements of CO_2 gas samples from June 2017 and January 2018.*

Sample number	Latitude (°N)	Longitude (°W)	$\delta^{13}C$-CO_2 ‰ (PDB)	Concentration CO_2 (ppm)	Description	Date collected
1	38.46982	112.85960	-9.997 ± 0.05	1,318.8 ± 43.2	Vegetation E of OMF	1/10/2018
2	38.49052	112.86332	-11.412 ± 0.05	637.1 ± 1.7	Vegetation W of OMF	1/12/2018
3	38.49865	112.89505	-12.079 ± 0.02	624.8 ± 0.01	FORGE vegetation	6/17/2017
4	38.39999	113.02161	-14.591 ± 0.03	587.1 ± 0.01	Regional vegetation	6/18/2017
5	38.47090	112.87240	-10.410 ± 0.03	583.3 ± 0.01	Vegetation W of OMF	6/25/2017
6	38.46222	112.88942	-11.924 ± 0.07	553.0 ± 0.4	Vegetation W of OMF	1/10/2018
7	38.49865	112.89505	-11.876 ± 0.11	549.2 ± 0.03	FORGE vegetation	1/13/2018
8	38.51275	112.92958	-11.331 ± 0.09	537.1 ± 0.04	Regional vegetation	1/13/2018
9	38.50056	112.89121	-12.966 ± 0.23	530.4 ± 0.02	FORGE vegetation	1/13/2018
10	38.51083	112.91233	-11.956 ± 0.03	507.6 ± 0.05	FORGE vegetation	6/17/2017
11	38.46569	112.95412	-12.92 ± 0.16	487.9 ± 0.09	Regional vegetation	1/14/2018
12	38.47019	112.86892	-10.268 ± 0.05	451.7 ± 0.0	Vegetation E of OMF	6/18/2017
13	38.46569	112.95412	-10.624 ± 0.11	417.0 ± 0.06	Air sample	1/14/2018
14	38.49865	112.89503	-10.635 ± 0.23	415.0 ± 0.04	Air sample	1/13/2018
15	38.47557	112.87965	-9.993 ± 0.03	409.0 ± 0.03	Air sample	6/18/2017

Helium Isotopic Composition

The majority of helium gas samples collected were not corrected for atmospheric contamination due to the high analytical error associated with correcting R/Ra values close to 1, as illustrated by the relatively high sigma value of 0.43 in sample 5 (R/Ra corrected = 1.19) (Table 3). For comparison, sample 13 has the highest corrected R/Ra value of 2.29 ± 0.06, representing an end-member composition. The four soil gas samples with elevated R/Ra (i.e., samples 4, 5, 6 and 13) have sufficiently high $^{4}He/^{20}Ne$ ratios to correct for air contamination, yielding values that range from R/Ra corrected = 1.19 to 2.29 (Table 3).

Table 3. *Helium isotope measurements on soil gases and a produced geothermal water.*

Sample	Elevation (m)	Latitude (°N)	Longitude (°W)	Setting	R/Ra	$^{4}He/^{20}Ne$	R/Ra corr
Diffusion samplers							
1	1680	38.49982	112.88811	Cold ground	0.98 ± 0.01	0.32 ± 0.01	---
2	1616	38.50782	112.89822	Cold ground	0.99 ± 0.01	0.33 ± 0.01	---
3	1633	38.51054	112.89820	Cold ground	1.00 ± 0.01	0.33 ± 0.01	---
4	1811	38.49818	112.85353	Hot steaming ground	1.42 ± 0.01	0.54 ± 0.01	2.03 ± 0.07
5	1855	38.49274	112.85237	Cold ground	1.01 ± 0.01	0.34 ± 0.01	1.19 ± 0.43
6	1814	38.48502	112.85885	Warm ground	1.13 ± 0.01	0.49 ± 0.01	1.37 ± 0.06
8	1675	38.47315	112.89625	Cold ground	0.99 ± 0.01	0.32 ± 0.01	---
9	1684	38.47303	112.89411	Cold ground	0.98 ± 0.01	0.32 ± 0.01	---
10	1795	38.46833	112.86491	Cold ground	1.02 ± 0.01	0.33 ± 0.01	---
11	1875	38.48771	112.84601	Cold ground	0.99 ± 0.01	0.31 ± 0.01	---
12	1737	38.47718	112.87658	Cold ground	1.00 ± 0.01	0.31 ± 0.01	---
13	1828	38.48997	112.85925	Warm ground	2.22 ± 0.01	5.95 ± 0.15	2.29 ± 0.06
Copper tube							
45-3		38.49062	112.85412	Production well	2.17 ± 0.01	30.20 ± 0.76	2.18 ± 0.06

DISCUSSION

Forge Site and West of the Opal Mound Fault

None of the 317 total individual CO_2 flux points measured across the FORGE site in June and January are greater than the calculated background flux thresholds when normalized for the instrumental error of 1% (Figure 6A). An interpolated flux map for the FORGE site and Opal Mound fault is shown in Figure 6A and Figure 6B. The main objective of this flux map is to determine where soil CO_2 flux is below the maximum threshold of biogenic values and where the flux is elevated above biogenic background. All of the green colors in Figures 6A and 6B represent CO_2 fluxes that are at (variance = 0) or below (variance less than zero) background. Figures 6A and 6B show that none of the interpolated flux measurements within the FORGE site are above calculated background values.

Just east of the FORGE site boundary, two point measurements are elevated above background outside the 1% error of the instrument. The highest flux of these points has a value of 12 ± 0.12 $gm^{-2}day^{-1}$ while the second point has a flux of 8.4 ± 0.08 $gm^{-2}day^{-1}$. Because these two points are discrete measurements surrounded by background values, the EBK flux map smooths out the slightly elevated higher values. These two values are aligned along a NW-SE line with one of the areas of high flux east of the Opal Mound fault. However, none of the other points measured along lines moving eastward are elevated above background until crossing the Opal Mound fault.

South of the FORGE site is a group of east and dominantly-west-dipping fault scarps that comprise the Mineral Mountains West fault (white lines in Figures 6A and 6B). This scarp system forms small grabens with a possible total offset in the overlying alluvium cover of less than 7 m (Knudsen et al., 2019). Four individual CO_2 flux point measurements elevated above background exist within this area. The highest flux measured in this area south of the FORGE site is 6.48 ± 0.064 $gm^{-2}day^{-1}$. This point is located along a line of three other points that may fall along a north-trending possible fault just south of the FORGE site.

Figures 7A and 7B show the isotopic composition and location of the 15 CO_2 gas samples collected across the FORGE site, the Opal Mound fault, and regionally (Figure 7B inset). The sample numbers used in Figure 7A correspond to Table 2 and Figure 7B. Shaded mixing regions have been drawn between average air $\delta^{13}C$ composition of the study area and typical global mantle (-6 ± 2.5‰; Sano and Marty, 1995), C4 vegetation, and C3 vegetation $\delta^{13}C$ compositions (Sharp, 2017). All of the soil gas samples inside the FORGE site clearly plot on average C4 vegetation-air or C3 vegetation-air mixing regions. This indicates that, in the FORGE site, all soil gas samples have a purely biogenic isotopic composition representative of the sage brush, desert grasses, and Juniper trees characterizing the vegetation across the area. Sample 3 was collected at flux point 569, the highest CO_2 flux point measured in June within the FORGE site with a value of 8.16 ± 0.082 $gm^{-2}day^{-1}$. This value

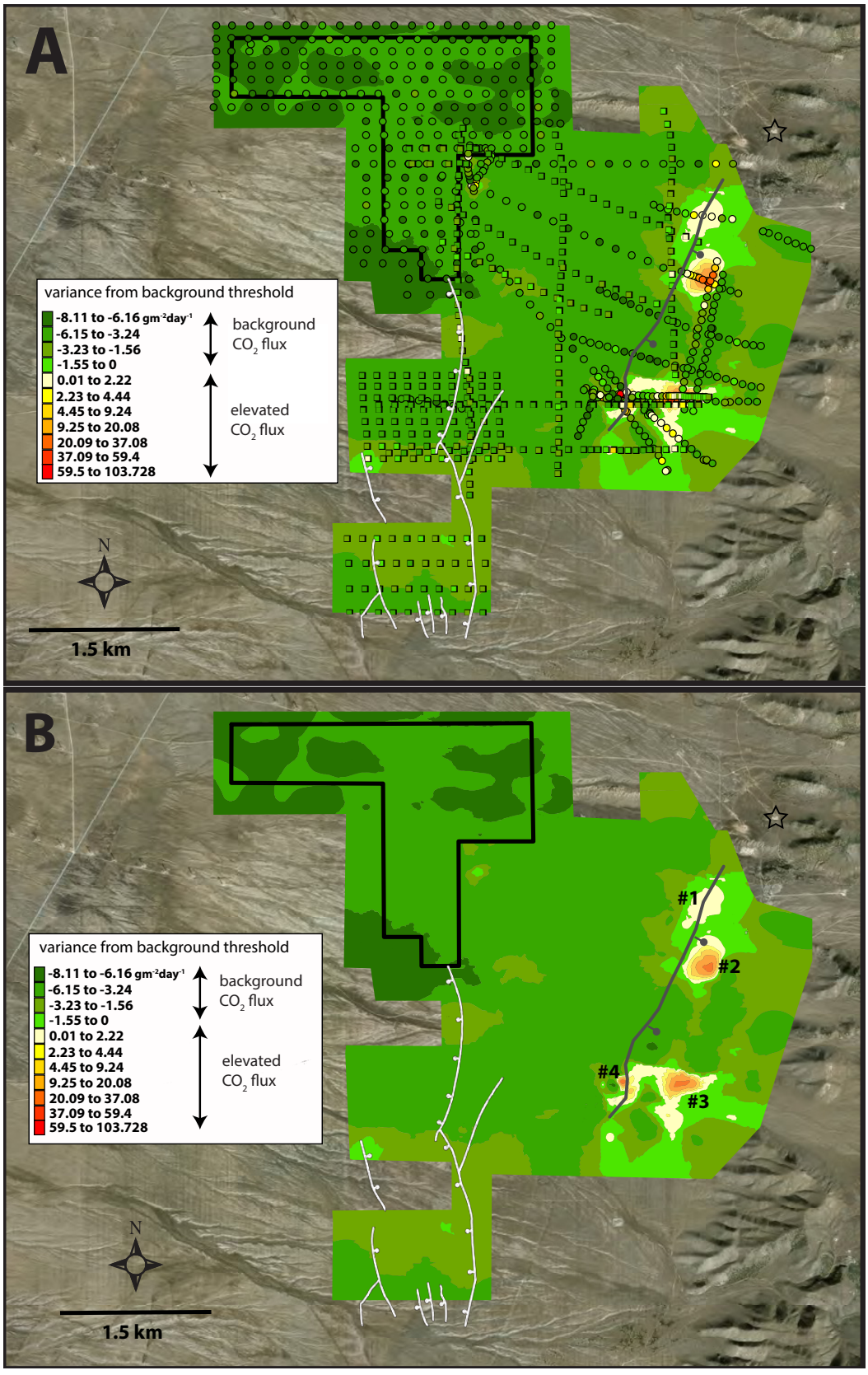

Figure 6. (A) *Empirical Bayesian Kriging flux map showing variance from background threshold overlain by individual point measurements of variance from background. Circle points are from June 2017 and square points are from January 2018.* ***(B)*** *Empirical Bayesian Kriging flux map showing variance from background threshold (individual point measurements removed for clarity). Regions #1, 2, 3, and 4 are elevated flux regions discussed in the text. FORGE site is the black polygon, Opal Mound fault is the dark gray line, scarps of the Mineral Mountains West fault are the white lines, and the black star is Roosevelt Hot Springs.*

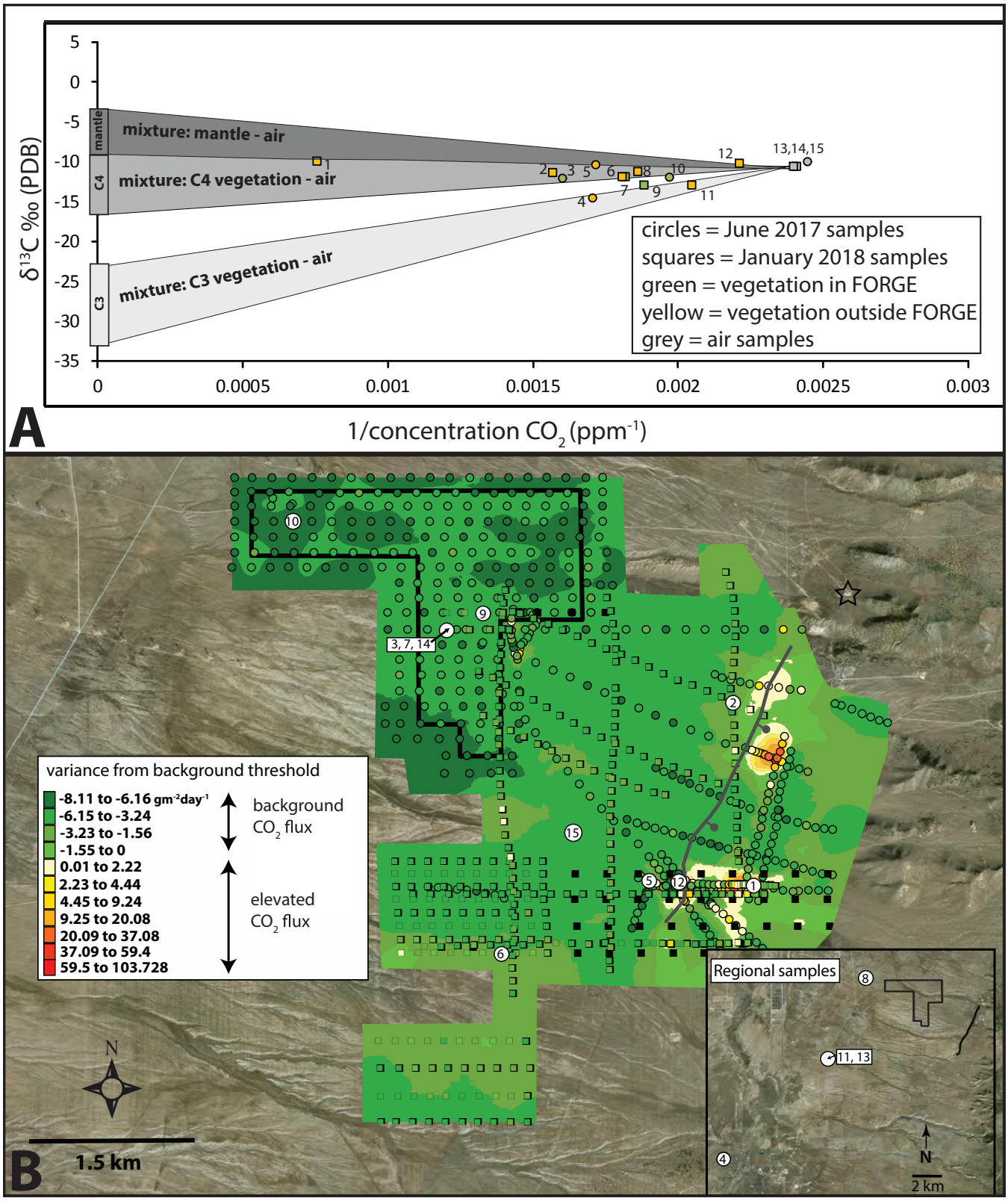

Figure 7. (A) *$\delta^{13}C$ composition versus 1/concentration for gas samples collected across the study area and regionally. Bars along the Y-axis indicate pure mantle (dark gray) (Sano and Marty, 1995), pure C4 vegetation (medium gray), and pure C3 vegetation (light gray) (Sharp, 2017). Shaded regions represent mixtures between air and end-member compositions. Sample numbers correspond to* ***(B)*** *Spatial distribution of gas samples across the FORGE site (black polygon), Opal Mound fault (dark gray line), Mineral Mountains West fault scarps (white lines), and regionally (inset) overlying Empirical Bayesian Kriging flux map of variance from background. Black star is Roosevelt Hot Springs.*

is just within the statistical background calculated for June when the 1% error of the instrument is considered. However, the $\delta^{13}C$ composition of point 569 lies well within the mixing region of C4 vegetation-air and therefore cannot be sourced from magmatic CO_2. This is also true for sample 6, collected from an elevated flux point along the Mineral Mountains West fault scarps south of the FORGE site.

Sample 6 also plots within the C4 vegetation-air mixing region and cannot be magmatically sourced. Gas sample 5 may be slightly heavier than the C4-air mixing region but has a low concentration, suggesting a purely biogenic source.

The isotopic composition of elevated flux values west of the Opal Mound fault suggests that the CO_2 source is not magmatic and therefore is sourced from near the surface rather than from rising hydrothermal fluids. This is consistent with the helium isotope analyses of soil gases. Furthermore, there is no evidence that the Mineral Mountains West fault scarps south of the FORGE site are pathways for deeply sourced CO_2.

East of the Opal Mound Fault

East of the Opal Mound fault, there are four regions (#1, #2, #3, and #4 in Figure 6B) of flux values elevated above background. These four regions are centered around the four highest individual flux values measured across the entire study area. Elevated flux region #1 intersects the northern sector of the Opal Mound fault, elevated flux region #2 is located approximately 1.5 km southwest of Roosevelt Hot Springs, elevated flux region #3 is located approximately 0.6 km east of the Opal Mound fault, and elevated flux region #4 intersects the southern portion of the Opal Mound fault. The highest individual CO_2 flux measurement within elevated region #2 is 50.16 $gm^{-2}day^{-1}$. The highest flux measurement within region #3 is 66.96 $gm^{-2}day^{-1}$. Elevated region #4 is located in soils directly adjacent to the siliceous sinter deposits of the Opal Mound fault and contains the highest flux value measured in the entire study area: 111.84 $gm^{-2}day^{-1}$. There is an additional region of elevated flux values along the northern trend of the Opal Mound fault, elevated region #1 (Figure 6B). However, the highest flux value for region #1 is much lower than the other three regions at only 11.52 $gm^{-2}day^{-1}$.

The only soil CO_2 gas samples that may possibly have a contribution of deeply-sourced, magmatic CO_2 are samples 1 and 12. Sample 1 was collected east of the Opal Mound fault in elevated region #3 where the measured flux was 2.55 $gm^{-2}day^{-1}$ in June 2017 and 0.45 $gm^{-2}day^{-1}$ in January 2018 with a $\delta^{13}C$ composition of -9.997‰. Even though sample 1 was collected in January when the overall CO_2 flux was lower, this gas sample has the highest concentration of all the samples collected (1,319 ppm). Furthermore, the isotopic composition of sample 1 may be heavier than the C4-air mixing region, suggesting a possible magmatic CO_2 component (Figure 7A). Soil gas sample 12 was collected from soil directly adjacent to the silica sinter on Opal Mound, and it appears to plot heavier than the C4-air mixing region (Figure 7A); however, the concentration of this particular sample is too close to the air-end member to resolve a magmatic CO_2 component with confidence.

The four soil gas samples with elevated R/Ra values over air (He soil gas samples 4, 5, 6, and 13) were collected east of the Opal Mound fault and represent mixtures in composition between air and thermal water collected from well 45-3 (Figures 8 and 9). Elevated R/Ra gas samples (13) and (6) were both collected within two of the previously discussed elevated CO_2 flux regions. No soil gas samples were collected for helium isotopic analysis within elevated flux region #4 intersecting the southern portion of the Opal Mound fault, where the highest soil CO_2 flux was measured (Figure 6B). However, in agreement with soil CO_2 data, the helium isotopic composition of all gas samples distinctly shows that R/Ra values elevated above air are located east of the Opal Mound fault. In summary, anomalous mantle helium is only detected in soil gases east of the Opal Mound fault and there is no evidence of mantle helium in samples from the vicinity of the FORGE site (Figure 9).

CONCLUSION

The FORGE prospective EGS site does not contain soil CO_2 flux values above statistical background, within analytical error. Soil CO_2 samples collected across the FORGE site have $\delta^{13}C$ compositions that plot with regional vegetation values along C3 vegetation-air or C4 vegetation-air mixing regions. At the intersection with and east of the Opal Mound fault, there are four regions of CO_2 flux elevated above background. The highest CO_2 flux values in these four regions vary from 11.52 to 111.84 $gm^{-2}day^{-1}$. Gas sample 1, collected from elevated region #3 east of the Opal Mound fault, may have a component of magmatic CO_2 based on $\delta^{13}C$ composition and CO_2 concentration. Gas sample 12, located at the intersection of the Opal Mound fault, may have a component of magmatic CO_2 as well but is too low concentration to determine with confidence. Elevated flux regions east of the Opal Mound fault are discrete and separated by regions of background flux values, suggesting that smaller-scale faults or fractures are creating pathways for deeply-sourced CO_2 to travel to the surface. The highest flux

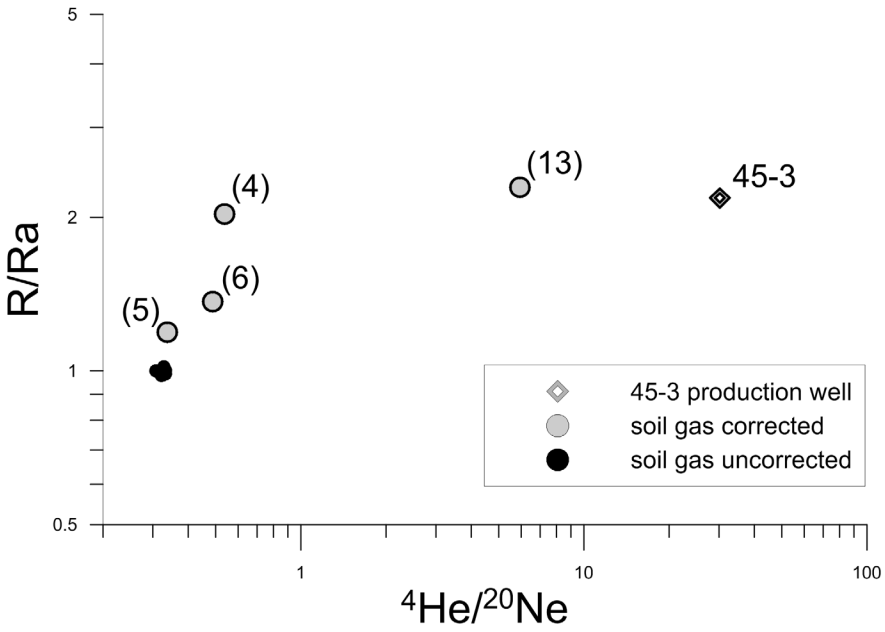

Figure 8. *R/Ra versus $^4He/^{20}Ne$ of soil gas samples collected across the FORGE site, Opal Mound fault, and Roosevelt Hot Springs region. Numbers in parentheses indicate sample sites shown in Figure 9.*

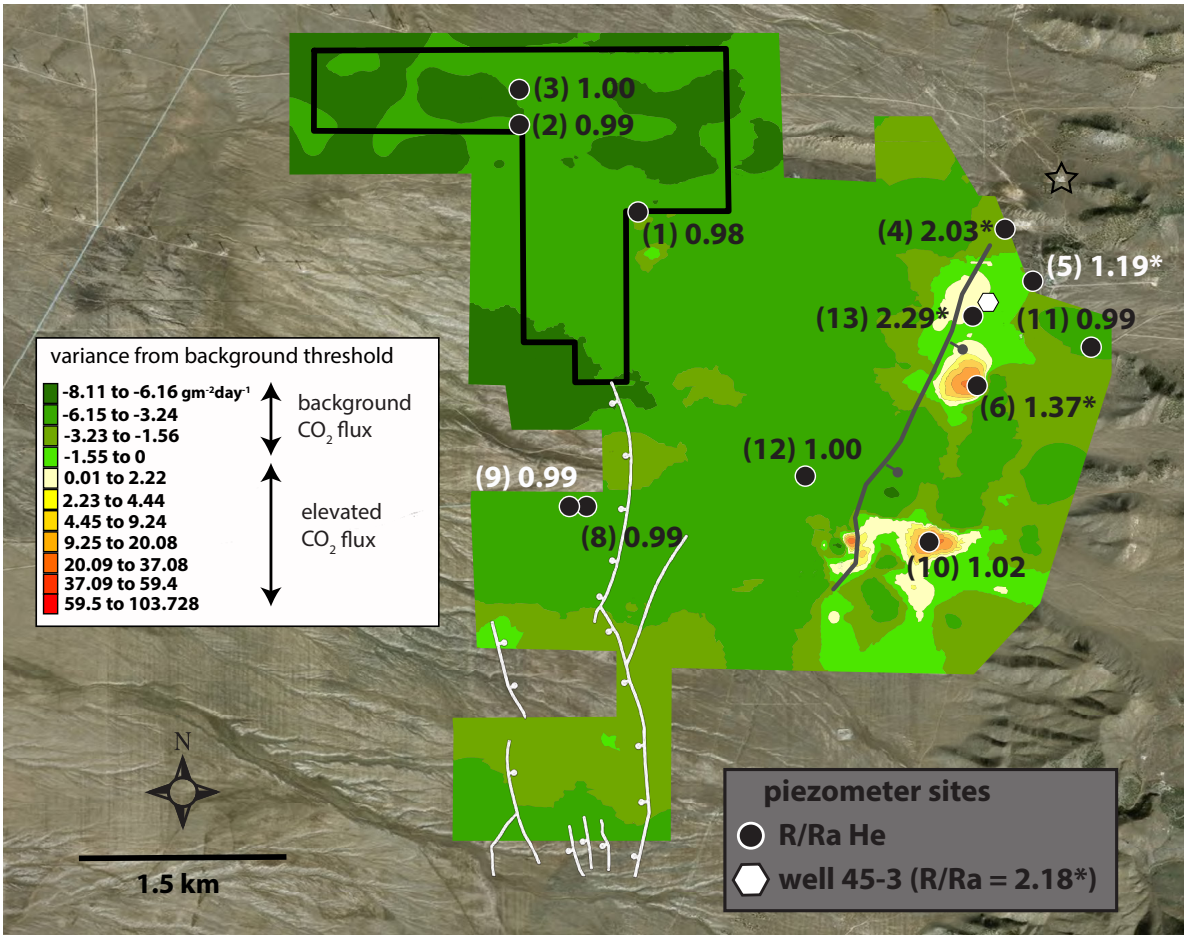

Figure 9. *Sample sites (black circles and white hexagon) with corresponding R/Ra helium isotope ratios overlying Empirical Bayesian Kriging flux map of variance from background. Asterisks indicate samples that have been corrected for air contamination. FORGE site is black polygon, Opal Mound fault is dark gray line, Mineral Mountains West fault scarps are white lines, and Roosevelt Hot Springs is the black star.*

value measured across the study area (111.84 $gm^{-2}day^{-1}$) was located on soils directly along the Opal Mound fault. However, the flow of deeply-sourced CO_2 appears to be centered around the remnants of siliceous sinter at the southern end of the fault, as flux values trending north along the fault return to background values. Soil gas samples with R/Ra values elevated above air are only located east of the Opal Mound fault. All samples collected within the FORGE site and west of the Opal Mound fault have air-like R/Ra values. Based on the spatial distribution of soil CO_2 flux, the $\delta^{13}C$ composition of soil CO_2, and the helium isotopic composition of soil gases, the Opal Mound fault serves as the western boundary of the Roosevelt Hot Springs system. Despite significant temperatures and thermal gradients, the Utah FORGE site has no evidence of deep-seated vertical gas permeability similar to the magmatic influences found east of the Opal Mound fault at Roosevelt Hot Springs.

ACKNOWLEDGMENTS

This work was sponsored by the DOE EERE Geothermal Technologies Office project DE-EE0007080 Enhanced Geothermal System Concept Testing and Development at the Milford City, Utah, FORGE Site. We thank Kent Smith for extensive field work assistance. We also thank Stefan Kirby and an anonymous reviewer for the reviews of an earlier draft of this report.

REFERENCES

Allis R.G., and Larsen, G., 2012, Roosevelt Hot Springs Geothermal field, Utah—reservoir response after more than 25 years of power production: Proceedings, 37th Workshop on Geothermal Reservoir Engineering, Stanford University, Stanford, California, 8p.

Allis, R., Moore, J., Davatzes, N., Gwynn, M., Hardwick, C., Kirby, S., McLennan, J., Pankow, K., Potter, S., and Simmons, S., 2016, EGS concept testing and development at the Milford, Utah FORGE site: Proceedings, 41st Workshop on Geothermal Reservoir Engineering, Stanford University, Stanford, California.

Bergfeld, D., Goff, F., and Janik, C.J., 2001, Elevated carbon dioxide flux at the Dixie Valley geothermal field, Nevada—relations between surface phenomena and the geothermal reservoir: Chemical Geology, v. 177, no. 1-2, p. 43–66.

Blackett, R.E., 2007, Review of selected geothermal areas in southwestern Utah: Geothermal Resources Council Transactions, v. 31, p. 111-116.

Chiodini, G., Cioni, R., Guidi, M., Raco, B., and Marini, L., 1998, Soil CO_2 flux measurements in volcanic and geothermal areas: Applied Geochemistry, v. 13, no. 5, p. 543–552.

Chiodini, G., Caliro, S., Cardellini, C., Avino, R., Granieri, D., and Schmidt, A., 2008, Carbon isotopic composition of soil CO_2 efflux, a powerful method to discriminate different sources feeding soil CO_2 degassing in volcanic-hydrothermal areas: Earth and Planetary Science Letters, v. 274, no. 3, p. 372–379.

Elberling, B., 2003, Seasonal trends of soil CO_2 dynamics in a soil subject to freezing: Journal of Hydrology, v. 276, no. 1-4, p. 159–175.

Faulder, D.D., 1991, Conceptual geologic model and native state model of the Roosevelt Hot Springs hydrothermal system: Proceedings, Sixteenth Workshop on Geothermal Reservoir Engineering, Stanford University, Stanford, California p 131–142.

Fischer, T.P., and Lopez, T.M., 2016, First airborne samples of a volcanic plume for $\delta^{13}C$ of CO_2 determinations: Geophysical Research Letters, v. 43, no. 7, p. 3272–3279.

Dame, B.E., Solomon, D.K., Evans, W.C., and Ingebritsen, S.E., 2015, Developing a new, passive diffusion sampler suite to detect helium anomalies associated with volcanic unrest: Bulletin of Volcanology, v. 77, no. 3, p. 1–17.

Gardner, P., and Solomon, D.K., 2009, An advanced passive diffusion sampler for the determination of dissolved gas concentrations: Water Resources Research, v. 45, no. 6, https://doi.org/10.1029/2008WR007399

Hardwick, C.L., Gwynn, M., Allis, R., Wannamaker, P., and Moore, J., 2016, Geophysical signatures of the Milford, Utah FORGE site: Proceedings, 41st Workshop on Geothermal Reservoir Engineering, Stanford University, Stanford, California.

Hardwick, C., Hurlbut, W., and Gwynn, M., 2019, Geophysical surveys of the Milford, Utah, FORGE site—gravity and TEM, *in* Allis, R., and Moore, J.N., editors, Geothermal characteristics of the Roosevelt Hot Springs system and adjacent FORGE EGS site, Milford, Utah: Utah Geological Survey Miscellaneous Publication 169-F, 15 p., https://doi.org/10.34191/MP-169-F.

Jones, C.G., Moore, J.N., and Simmons, S., 2019, Petrography of the Utah FORGE site and environs, Beaver County, Utah, *in* Allis, R., and Moore, J.N., editors, Geothermal characteristics of the Roosevelt Hot Springs system and adjacent FORGE EGS site, Milford, Utah: Utah Geological Survey Miscellaneous Publication 169-K, 23 p., 2 appendices, https://doi.org/10.34191/MP-169-K.

Kennedy, B.M., and van Soest, M.C., 2007, Flow of mantle fluids through the ductile lower crust: Helium isotope trends: Science, v. 318, no. 5855, p. 1433–1436.

Knudsen, T., Kleber, E., Hiscock, A., and Kirby, S.M., 2019, Quaternary geology of the Utah FORGE site and vicinity, Millard and Beaver Counties, Utah, *in* Allis, R., and Moore, J.N., editors, Geothermal characteristics of the Roosevelt Hot Springs system and adjacent FORGE EGS site, Milford, Utah: Utah Geological Survey Miscellaneous Publication 169-B, 21 p., 2 appendices, https://doi.org/10.34191/MP-169-B.

Krivoruchko, K., 2012, Empirical bayesian kriging: Esri, Redlands, California, USA.

Lee, H., Muirhead, J., Fischer, T., Ebinger, C., Kattenhorn, S., and Kianji, G., 2016, Tectonic degassing of mantle-derived CO_2 along faults in the East African Rift: Nature Geoscience, v. 9, p. 145–149.

Lewicki, J.L., Evans, W.C., Hilley, G.E., Sorey, M.L., Rogie, J.D., and Brantley, S.L., 2003, Shallow soil CO_2 flow along the San Andreas and Calaveras faults, California: Journal of Geophysical Research, Solid Earth, v. 108, no. B4, p. 14.

Lewicki, J.L. and Oldenburg, C.M., 2005, Near-surface CO_2 monitoring and analysis to detect hidden geothermal systems: Proceedings, Thirteenth Workshop on Geothermal Reservoir Engineering, Stanford University, Stanford, California.

Lewicki, J.L., Bergfeld, D., Cardellini, C., Chiodini, G., Granieri, D., Varley, N., and Werner, C., 2005, Comparative soil CO_2 flux measurements and geostatistical estimation methods on Masaya volcano, Nicaragua: Bulletin of Volcanology, v. 68, no. 1, p. 76–90.

Lynne, B.Y., Campbell, K.A., Moore, J.N., and Browne, P.R.L., 2005, Diagenesis of 1900-year-old siliceous sinter (opal-A to quartz) at Opal Mound, Roosevelt Hot Springs, Utah, USA: Sedimentary Geology, v. 179, no. 3, p. 249–278.

Miller, J., Allis, R., and Hardwick, C., 2019, Interpretation of seismic reflection surveys near the FORGE enhanced geothermal systems site, Utah, *in* Allis, R., and Moore, J.N., editors, Geothermal characteristics of the Roosevelt Hot Springs system and adjacent FORGE EGS site, Milford, Utah: Utah Geological Survey Miscellaneous Publication 169-H, 13 p., https://doi.org/10.34191/MP-169-H.

Moore, J.N., and Nielson, D.L., 1994, An overview of the geology and geochemistry of the Roosevelt Hot Springs geothermal system, Utah: Utah Geological Association Publication, v. 23, p. 25–36.

Nielson, D.L., Evans, S.H., and Sibbett, B.S., 1986, Magmatic, structural, and hydrothermal evolution of the Mineral Mountains intrusive complex, Utah: Geological Society of America Bulletin, v. 97, p. 765–777.

Ozima, M., and Podosek, F.A., 1983, Noble gas geochemistry: Cambridge University Press, 367 p.

Parks, M.M., Caliro, S., Chiodini, G., Pyle, D.M., Mather, T.A., Berlo, K., Edmonds, M., Biggs, J., Nomikou, P., and Raptakis, C., 2013, Distinguishing contributions to diffuse CO_2 emissions in volcanic areas from magmatic degassing and thermal decarbonation using soil gas ^{222}Rn–$\delta^{13}C$ systematics—Application to Santorini volcano, Greece: Earth and Planetary Science Letters, v. 377, p. 180–190.

Peiffer, L., Bernard-Romero, R., Mazot, A., Taran, Y.A., Guevara, M., and Santoyo, E., 2014, Fluid geochemistry and soil gas fluxes (CO_2–CH_4–H_2S) at a promising Hot Dry Rock Geothermal System—The Acoculco caldera, Mexico: Journal of Volcanology and Geothermal Research, v. 284, p. 122–137.

PP Systems, 2016, EGM-5 Portable CO_2 Gas Analyzer Operation Manual, Version 1.01, Amesbury, Massachusetts.

Rizzo, A.L., Jost, H.J., Caracausi, A., Paonita, A., Liotta, M., and Martelli, M., 2014, Real-time measurements of the concentration and isotope composition of atmospheric and volcanic CO_2 at Mount Etna (Italy): Geophysical Research Letters, v. 41, no. 7, p. 2382–2389.

Sanford, W., Shropshire, R., and Solomon, D., 1996, Dissolved gas tracers in groundwater—Simplified injection, sampling, and analysis: Water Resources Research, v. 32, no. 6, p. 1635–1642.

Sano, Y., and Marty, B., 1995, Origin of carbon in fumarolic gas from island arcs: Chemical Geology, v. 119, no. 1–4, p. 265–274.

Sharp, Z., 2017, Principles of stable isotope geochemistry, 2nd Edition, Albuquerque, University of New Mexico, doi:10.5072/FK2GB24S9F.

Simmons, S., Kirby, S., Moore, J., Wannamaker, P., and Allis, R., 2015, Comparative analysis of fluid chemistry from Cove Fort, Roosevelt and Thermo: Implications for geothermal resources and hydrothermal systems on the east edge of the Great Basin: 39th Geothermal Resources Council Annual Meeting-Geothermal: Always On, GRC 2015, Reno, Nevada.

Simmons, S.F., Moore, J.N., Allis, R., Kirby, S., Jones, C., Bartley, J., Kleber, E. Tyler, K., Milller, J., Hardwick, C., Rahilly, K., Gwynn, M., McLennan, J., Forbes, B., Podgorney, R., Pankow, K., Wannamaker, P., and Fischer, T., 2018, A revised geoscientific model of the FORGE Utah EGS laboratory: Proceedings, 43rd Workshop on Geothermal Reservoir Engineering, Stanford University, Stanford, California.

Sinclair, A.J., 1974, Selection of threshold values in geochemical data using probability graphs: Journal of Geochemical Exploration, v. 3, no. 2, p. 129–149.

Wannamaker, P.E., Faulds, J. E., and Kennedy, B.M., 2017, Integrating magnetotellurics, soil gas geochemistry and structural analysis to identify hidden, high enthalpy, extensional geothermal systems: University of Utah/EGI Technical Report to U.S. Department of Energy, Office of Energy Efficiency & Renewable Energy Geothermal Technologies Program.

Werner, C., and Brantley, S., 2003, CO_2 emissions from the Yellowstone volcanic system: Geochemistry, Geophysics, Geosystems, v. 4, no. 7, 27p.

Western Regional Climate Center – Desert Research Institute: Reno, Nevada Online, https://cemp.dri.edu/cgi-bin/cemp_stations.pl?stn=milu, accessed January 18, 2018.